Supporting Information

Multilevel Composite using Carbon Nanotube Fibers (CNTF)

XiaoMeng Sui[a,*,‡], Israel Greenfeld[a,*,‡], Hagai Cohen[b], XiaoHua Zhang[c], QingWen Li[c], and H. Daniel Wagner[a,*]

[a]*Department of Materials and Interfaces, Weizmann Institute of Science, Rehovot 76100, Israel*

[b]*Chemical Research Support, Weizmann Institute of Science, Rehovot 76100, Israel*

[c]*Suzhou Institute of Nano-Tech and Nano-Bionics, Suzhou 215123, China*

‡These authors contributed equally to this work.

*Corresponding authors

E-mail addresses:

xiaomeng.sui@weizmann.ac.il (X. Sui)

green_is@netvision.net.il (I. Greenfeld)

Daniel.Wagner@weizmann.ac.il (H.D. Wagner)

S1. Fragmentation test and data analysis

Fragmentation test. In a fragmentation test, the CNTF breaks gradually due to the stress transferred via the epoxy-CNTF interface, until the fragmentation reaches saturation. Due to the nature of the fragmentation test, a successful test requires two pre-conditions: i. the ultimate tensile strain of the fiber should be much smaller than that of the matrix; ii. the interface between the two components should be relatively good. After solvent-infiltration treatment, the CNTFs show shorter elongations and higher Young's moduli and strengths, compared to those of untreated fibers. It is believed that the treatment with solvent/solution densifies the assembly structure, thus improving the adhesion between CNTs in a bundle and/or between the bundles in a CNTF. The result is less CNT-CNT or bundle-bundle sliding when the CNTF is under tension, and the fiber will show improved strength and modulus. This finding is similar to independent research, when a different solvent/polymer was introduced to densify the CNTFs [1-3].

The epoxy resin chosen in this work has a relatively long elongation, about 18% at a slow stretching speed (0.01 mm/min) at room temperature. The as-spun CNTF without any treatment has about 9%-10% ultimate tensile strain, which is not significantly different from epoxy, compared to the two treated CNTFs. Indeed the fragmentation test of as-spun (untreated) CNTF was not successful, and therefore there is no test result for this sample. The critical lengths are more than 10 times longer than the fiber diameter, so that the shear stress can reach its maximum value, and the CKT model remains valid. See also information in Supporting Information section S2 about thermal residual stresses induced during epoxy curing, and how the stress calculation is corrected accordingly.

The continuously monitored single-fiber fragmentation tests were performed on a Minimat tensile tester equipped with a 200N load cell, with deformation speed at 0.05 mm/min. The tensile tester was mounted on a microscope equipped with polarized light so that the whole process could be accurately monitored. The experiment was recorded by a CCD camera attached to the microscope for later analysis. The video and the test were synchronized, so that the stress level of the matrix could be known when fiber breaks happen. Because the CNTFs had about 60 breaks in each sample, it was impossible to scan the whole specimen and count the breaks. We fixed the lens in the middle of the specimen, and assumed the middle part is representative for the whole specimen. The process of the fragmentation test, *i.e.* the correlation between the number of breaks and the stress level, was monitored and recorded for the part of the fiber within the CCD

camera view field. See CNTF fragmentation video in Supporting Information. Upon saturation, when the interfacial shear stress cannot further break the fiber, the total number of breaks of the whole fiber was counted by scanning the fiber.

Data analysis. In order to calculate the interfacial shear strength τ using the CKT model (Equation (2) in the main text), the fiber diameter *D* was measured under a scanning electron microscope, and its critical length l_c was taken as 4/3 of the average fragment length when the fragmentation reached saturation [4]. Note that the standard CKT model assumes a solid fiber with a circular interfacial perimeter, whereas a CNTF consists of hollow CNTs and CNT bundles, and contains voids between the CNTs as well as polymer matrix that penetrated during the packaging process. Therefore, the calculated values of τ and $\sigma_f(l_c)$ should be regarded as apparent values rather than actual material strengths. This issue is discussed in detail in the main text, including a suggestion for model adjustment.

For the average fragment length, we used a sample gauge length divided by the number of breaks plus one (n+1). For most fibers, the critical length is less than 1 mm, and the measurement of strength of such short fibers is beyond the technical capability in most research labs. A traditional way to extrapolate and obtain the strength of fibers at the critical length is to test the strength of the fiber at different gauge lengths, and then to express the exponential relationship between the mean fiber strength and the fragment length using the Weibull distribution [5]. This method requires a large number of samples and tests.

To avoid such an approach, we used a continuously monitored fragmentation test [6], and fitted the results to the reverse form of the Weibull distribution:

$$\bar{l} = \alpha^{\beta} \bar{\sigma}_{f\infty}^{-\beta} \left[\Gamma\left(1+\beta^{-1}\right)\right]^{\beta}, \qquad \text{(S1)}$$

where $\bar{l}$ and $\bar{\sigma}_{f\infty}$ are the mean length and strength of fragments at each step of the test, and $\Gamma(\ )$ is the Gamma function. α and β are the Weibull scale and shape parameters for the strength of the embedded fiber, respectively. As far as the test is not reaching saturation, a ln-ln plot of equation (S1) is a straight line whose slope equals the negative value of the Weibull shape parameter (-β). The scale parameter α is calculated from the line's intercept. The Weibull scale parameter α provides the predictable strength of the fiber, while the shape parameter β is an

indicator for the fiber strength variability (higher β values mean lower strength variability) and hence the fiber reliability. The resulting Weibull probability densities of the fiber strength, based on the extracted values of α and β, are depicted in Figure 4 in the main text.

S2. Calculation of fiber stress

Measurements of the fiber and matrix tensile moduli allow calculation of the fiber stress transferred via its matrix interface, so long as the fragmentation is sufficiently far from saturation. We use the following iso-strain relationship for a fiber embedded longitudinally in a matrix:

$$\frac{\sigma_f}{\sigma_m} = \frac{E_f}{E_m}, \tag{S2}$$

in which σ and E are stress and modulus, and the subscripts f and m stand for fiber and matrix, respectively.

We noticed that during sample preparation, due to negative thermal expansion and epoxy shrinkage when chemically cured, the fiber suffers a compressive residual stress. To avoid fiber buckling, we applied pre-stress on the fiber. Thus, the far-field fiber stress is expressed by:

$$\sigma_{f\infty} = \sigma_m \frac{E_f}{E_m} - \sigma_f^{th} - \sigma_m^{cure} + \sigma_{pre}, \tag{S3}$$

where σ_f^{th} $\sigma_{\mathbf{f}}^{\mathbf{th}}$ is the residual thermal stress caused by temperature changes [7-8], σ_m^{cure} is the stress cause by epoxy shrinkage, and σ_{pre} is the stress induced by the pre-stress. σ_f^{th} can be calculated from a simple one-dimensional model:

$$\sigma_f^{th} = \left(\alpha_{Lm} - \alpha_{Lf}\right)\left(T_{ref} - T\right)\frac{E_f}{1 + \frac{\varphi_f}{\varphi_m}\frac{E_f}{E_m}}, \tag{S4}$$

where α_L is the coefficient of thermal linear expansion (CTE), T is room temperature, and T_{ref} is the curing temperature.

The following example demonstrates this calculation for the CNTF(EG)-epoxy sample. Since the fiber and the epoxy have the same length in the sample, the ratio between their volume fractions (φ) is the same as the ratio between their cross sectional areas (A):

$$\frac{\varphi_f}{\varphi_m}=\frac{A_f}{A_m}=\frac{\pi\left(\frac{1}{2}D\right)^2}{tw}=\frac{\pi\left(\frac{1}{2}14.5\cdot10^{-6}\right)^2}{1\cdot10^{-3}\cdot1.5\cdot10^{-3}}=1.10\cdot10^{-4}, \qquad \text{(S5)}$$

where *t* and *w* are the sample thickness and width, respectively. The measured Young's moduli of the CNTF(EG) and the matrix are 33.9 GPa and 0.7 GPa, repectively (Table 1 in the main text). The coefficients of thermal linear expansion for epoxy and CNT are estimated as $136\cdot10^{-6}$ $^{o}C^{-1}$ and $20\cdot10^{-6}$ $^{o}C^{-1}$, respectively [8-10]. Since the CTE value for the CNTF is not known, we use instead the value for the double-walled CNTs used for winding the CNTF. The thermal stress is then (equation (S4)):

$$\sigma_f^{th}=(136-20)10^{-6}(100-25)\frac{33.9\cdot10^3}{1+1.1\cdot10^{-4}\frac{33.9}{0.7}}=293.4\,\text{MPa}. \qquad \text{(S6)}$$

Assuming $\varepsilon_m=1\%-2\%$ epoxy shrinkage due to chemical curing [11], the curing stress is:

$$\sigma_m^{cure}=E_m\varepsilon_m=0.7\cdot10^3\cdot0.01=7.0\,\text{MPa}. \qquad \text{(S7)}$$

A fishing bead ($F=0.5\,\text{g}$) was attached to each fiber during sample preparation, resulting in a pre-stress of:

$$\sigma_{pre}=\frac{F}{A_f}=\frac{0.5\cdot10^{-3}\cdot9.8}{\pi\left(\frac{1}{2}14.5\cdot10^{-6}\right)^2}10^{-6}=29.7\,\text{MPa}. \qquad \text{(S8)}$$

It can be seen that the residual thermal stress is significant, and is dominant over the epoxy curing stress. Although the pre-stress applied on the CNTF is small compared to the thermal stress, it ensures straight laying of the fiber during curing and avoiding buckling. Finally, the far-field fiber stress in the CNTF(EG) fiber is calculated by (equation (S3)):

$$\sigma_{f\infty}=\sigma_m\frac{E_f}{E_m}-270.7\,\text{MPa}. \qquad \text{(S9)}$$

Similarly, the far-field fiber stress in the CNTF(HNO_3) fiber is calculated by:

$$\sigma_{f\infty}=\sigma_m\frac{E_f}{E_m}-280.1\,\text{MPa}. \qquad \text{(S10)}$$

S3. Revised CKT model

As described in the main text, The CKT model in equation (1) assumes a circular solid fiber with external diameter D. However, the CNTF consists of hollow CNTs, assembled tightly into bundles, in turn assembled loosely into a fiber, with gaps between CNTs as well as penetrated interphase between bundles. In this section we present, based on our previous work on CNT bundles [12], a revised CKT model that accounts for this intricate structure, including the concept of effective diameter. We make a distinction between tight packing, representative of a bundle structure, and loose packing, representative of a CNTF structure (Figure 5 in the main text).

In *tightly packed CNTFs* (Figure 5a in the main text), the CNTF-epoxy interface exists only at the external surface of the outermost CNTs exposed to the matrix. Bundling of CNTs is ignored in this hypothetical conformation. We first calculate the actual CNTF interfacial perimeter p (the contact area marked by the thick line in Figure 5a in the main text) and the material cross-sectional area a (the cumulative material cross-sectional area of all CNTs in a CNTF cross section) of a tightly packed CNTF with an external diameter D. The CNTF boundary consists of a string of nearly half circles (Figure 5a in the main text), and therefore p is (approximately) augmented by a factor of $\pi/2$ (regardless of the circles radii) with respect to the perimeter of a perfectly circular fiber p_{CNTF} [12]:

$$\frac{p}{p_{CNTF}} \cong \frac{\frac{1}{2}\pi d}{d} \cong \frac{\pi}{2}. \qquad \text{(S11)}$$

where d is the external diameter of a single CNT.

Voids are present inside the hollow CNTs, as well as between the CNTs, and therefore a is decreased (by a factor that depends on the CNT diameter and wall thickness) with respect to the area of a perfectly circular fiber. Considering a representative triangle connecting the centers of three hexagonally packed CNTs, the actual material cross-sectional area a of the CNTF is decreased with respect to the CNTF total area a_{CNTF} by the ratio between the CNTs material area enclosed by the triangle and the triangle area, given by [12]:

$$\frac{a}{a_{CNTF}} \cong \frac{\frac{1}{2}a_{CNT}}{\frac{\sqrt{3}}{4}d^2} \cong \frac{2\pi}{\sqrt{3}}\frac{t}{d}\left(1-\frac{t}{d}\right), \qquad \text{(S12)}$$

where t is the wall thickness of a single CNT. If the CNT diameter and/or wall thickness are unknown, the CNTF material cross sectional area can be derived by

$$\frac{a}{a_{CNTF}} \cong \frac{\rho_{CNTF}}{\rho_{CNT}}, \qquad \text{(S13)}$$

where ρ_{CNT} is the CNT material density, and ρ_{CNTF} is the CNTF apparent density including voids. The CNTs used in our experiment are mostly double-walled, having average $d \cong 7.5$ nm and $t \cong 1$ nm, and therefore the CNTF actual material cross sectional area is lower by a factor of $a / a_{CNTF} \cong 0.42$ with respect to the CNTF total area (equation (S12)). By comparison, given $\rho_{CNTF} = 1.07$ g/cm^3 from the manufacturer data and $\rho_{CNT} = 2.1$ g/cm^3, we get $a / a_{CNTF} \cong 0.51$ (equation (S13)).

Substituting these factors into the standard CKT model of equation (1) in the main text, and assuming perfect stress transfer between CNTs, we obtain the adjusted model for a tightly packed CNTF [12]:

$$\tau = \frac{\sigma_f}{2l_c}\frac{4a}{p} \cong \frac{\sigma_f D}{2l_c} C_{td}, \quad \text{where} \quad C_{td} \equiv \frac{4}{\sqrt{3}}\frac{t}{d}\left(1-\frac{t}{d}\right), \qquad \text{(S14)}$$

in which σ_f and τ are the CNTF actual tensile and interfacial material strengths. The dimensionless correction factor C_{td} is a function of the geometry, and is monotonically rising with the cross sectional aspect ratio t/d. It ranges from 0 for a thin wall CNT ($t << d$) to ~0.58 for a solid CNT (not tubular, $t = d/2$). Note the use of the term $4a/p$, which reduces to D for a solid circular filler. This term is universal for any cross sectional cylindrical geometry, and takes into account both the material area bearing the tensile stress, and the actual CNTF-matrix contact area bearing the interfacial stress. If the stress transfer between CNTs is not perfect, the area a will be effectively smaller, resulting in smaller C_{td}.

In view of the larger interfacial perimeter, the actual τ is smaller by a factor of $\pi/2 = 1.57$ compared to the value derived from measurements in Table 2 in the main text. Similarly, in view of the smaller material cross sectional area, the actual σ_f is larger by the ratio between the CNTF total cross sectional area and the CNTF material cross-sectional area, a_{CNTF}/a. As calculated above for the specimens used in our experiment, $a / a_{CNTF} \cong 0.42$ and

therefore the actual σ_f is larger by a factor of $1/0.42 = 2.39$. These actual material interfacial and tensile strengths estimates for tightly-packed CNTFs are compared in Table 3 in the main text with the values derived by the standard CKT estimates, and with typical published measurements of σ_f of a single MWCNT [13-14] and τ of a single MWCNT embedded in epoxy [15-18]. τ drops from 73.9 MPa (EG) and 40.6 MPa (HNO_3), when calculated with the standard CKT model, to 47.0 MPa (EG) and 25.8 MPa (HNO_3) when adjusted to the tight packing model (equation (S14)). Similarly, σ_f jumps from 2.7 GPa (EG) and 3.5 GPa (HNO_3), when calculated with the standard CKT model, to 6.5 GPa (EG) and 8.4 GPa (HNO_3) when adjusted to the tight packing model. These are indeed large differences, which result solely from simple geometrical considerations. These estimates are only presented for reference, since our experimental observations have shown polymer penetration in both sample types, particularly for the EG treated CNTF but also to some extent for the HNO_3 treated CNTF. Therefore, together with the assumption of perfect stress transfer between CNTs, the condition of perfect tight packing is only hypothetical.

In *loosely packed CNTFs* (Figure 5b in the main text), due to penetration of matrix material into the CNTF, filling the gaps between CNT bundles, the CNT-matrix contact perimeter p increases further (the thick line in Figure 5b in the main text). The CNTF material cross section a remains essentially unchanged (since the number of CNTs comprising the CNTF does not change), but the mechanism of stress transfer from the outer CNTs to the inner ones is different. In a tightly packed CNTF, the stress propagates by inter-CNT forces along contact lines, and we assumed uniform tensile stress throughout a cross-section. By contrast, in a loosely packed CNTF, the inter-CNT forces are smaller because of larger gaps between CNTs, but, on the other hand, the stress is transferred by the matrix interphase via larger contact areas. Hence, the area a may change further (increase or decrease), depending on the effectiveness of the stress transfer. The net effect on the actual interfacial strength is determined by the ratio a/p.

Equation (S14) can be generalized for an arbitrary cross sectional geometry and interphase size, by defining an effective CNTF diameter $\langle D \rangle$ [12]:

$$\tau = \frac{\sigma_f \langle D \rangle}{2l_c}, \quad \langle D \rangle \equiv \frac{4a}{p}, \tag{S15}$$

where, as before, σ_f and τ are the CNTF actual tensile and interfacial material strengths. This form has the advantage of using the standard CKT model, except that D is replaced by $\langle D \rangle$. Furthermore, since the tensile and interfacial strengths are actual strengths, they can be assessed against known material values from the literature. Such assessment is impractical when effective strengths are considered, since those vary with the CNTF specific nano geometry and degree of densification.

The effective diameter for a tightly packed CNTF can be obtained from equation (S14):

$$\langle D \rangle_{\text{tight}} = C_{td} D, \tag{S16}$$

and for the multiwall CNT geometry of our experiment $\langle D \rangle_{\text{tight}} = 0.267D$, using the average values $d \cong 7.5$ nm and $t \cong 1$ nm. In case the CNT diameter and/or wall thickness are unknown, the material cross sectional area is decreased by the ratio ρ_{CNT} / ρ_{CNTF} (equation (S13)). Hence, in that case, $\langle D \rangle_{\text{tight}}$ can be calculated by:

$$\langle D \rangle_{\text{tight}} = \left(\frac{2}{\pi} \frac{\rho_{CNTF}}{\rho_{CNT}} \right) D. \tag{S17}$$

Given $\rho_{CNTF} = 1.07$ g/cm^3 (EG-treated) and $\rho_{CNT} = 2.1$ g/cm^3, we get $\langle D \rangle_{\text{tight}} = 0.324D$, where the values of D are given in Table 2 in the main text.

It is convenient to define a dimensionless polymer penetration factor

$$P \equiv 1 - \frac{\langle D \rangle}{\langle D \rangle_{\text{tight}}} = 1 - \frac{\langle D \rangle}{D} C_{td}^{-1}, \tag{S18}$$

which equals 0 for zero penetration, and increases toward 1 for growing penetration. The limit of 1 is approached when the CNT bundles are completely separated from each other by surrounding matrix, thus vastly increasing the interfacial perimeter p in equation (S15). Inverting equation (S18), the effective CNTF diameter can be expressed in terms of the product of the geometric factor C_{td}, the penetration factor P, and the CNTF external diameter D:

$$\langle D \rangle = (1 - P) \langle D \rangle_{\text{tight}} = C_{td} (1 - P) D. \tag{S19}$$

These concepts are captured in Table 3 in the main text and in Figure S1, for the experimental results of this study, and using the actual σ_f for tight packing. The tight packing estimates for τ in Table 3 in the main text assume perfect hexagonal packing, in other words a zero polymer penetration factor. As observed in our experiments, polymer penetration is more pronounced in the EG-treated CNTF, compared to the HNO_3-treated CNTF (Figure 2 in the main text). In the HNO_3-treated CNTFs we observed a little penetration, with an estimated penetration factor of 0.1 ± 0.1, reducing τ from 25.8 MPa for tight packing (*i.e.*, no penetration)) to 22.9 MPa (equations (S15) and (S19)). Taking this value as the matrix material property, and assuming the same actual τ in both treatment cases (namely 22.9 MPa), the polymer penetration factor for the EG-treated CNTFs can be estimated to be about 0.5 ± 0.1, and the actual τ is reduced accordingly from 47.0 MPa for tight packing to 22.9 MPa. In this way, the actual strengths of the fiber and interface are comparable with known material properties in Table 3 in the main text, whilst the observed substantial polymer penetration is reflected in the penetration factor. Calculating in reverse, the actual interfacial strengths can be obtained by applying a factor of $C_{td}(1-P)/(C_{td}\pi/2)$ or $2(1-P)/\pi$ to their respective effective values.

It should be noted that the assumption of same actual τ is taken in the absence of direct interfacial measurements, realizing that it should be somewhat lower in the HNO_3-treated CNTF, where matrix yield was not observed as in the EG-treated CNTF. These estimates are denoted by the loose packing values in Table 3 in the main text, and are illustrated by the thick red lines in Figure S1. Comparing on the basis of the same cross sectional area, this means that the interfacial area grew by factors of $1/(1-0.1) \cong 1.1$ (HNO_3) and $1/(1-0.5) = 2$ (EG) with respect to a perfect tightly packed CNTF.

The benefit from the concept of effective diameter $\langle D \rangle$ is in the use of actual strengths of the CNT (σ_f) and the CNT-matrix interface (τ), which are inherent material properties, rather than using values that vary with internal geometry. These varying conditions are now incorporated into $\langle D \rangle$, which accounts for all the voids inside the CNTF, as well as for the increase in load bearing interfacial area and the efficiency of stress transfer between the CNTs inside the CNTF. $\langle D \rangle$ should be significantly smaller than D in most cases. While this may seem counter-intuitive at first glance, remember that, with respect to a filler with a solid circular

cross section, the CNTF's interfacial perimeter p is longer due to surface roughness and polymer penetration, whereas its material cross section a is smaller due to voids.

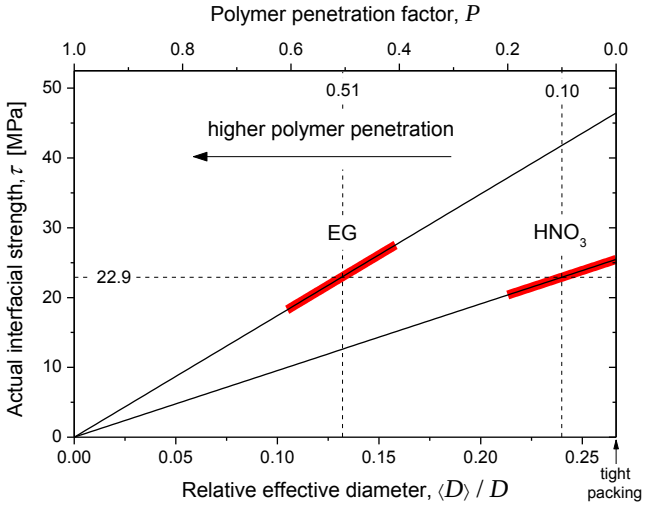

Figure S1. Estimation of polymer penetration in loose packing. The actual interfacial strength τ is expressed in terms of the relative effective diameter $\langle D \rangle / D$ and the polymer penetration factor P (equation (S18)), where D is the CNTF external diameter, and $\langle D \rangle$ is the CNTF effective diameter. The EG and HNO_3 lines are plotted with equation (S15), using the data from Table 2 and Table 3 in the main text. The thick red regions mark the estimated penetration ranges for the EG and HNO_3 test groups. The mean value of τ (22.9 MPa) is assumed to be the same for both CNTF types (Table 3 in the main text).

To summarize, according to this analysis, the estimated actual (*i.e.*, intrinsic) interfacial strengths for both solvent treatments are assumed similar, since both are basically a material property of the same matrix, while the effective (*i.e.*, apparent) interfacial strength is much higher in the EG-treated CNTF due to higher polymer penetration. The effective diameters in both treatments are similar, 1.9 μm for the CNTF(EG) and 1.7 μm for the CNTF(HNO_3), and since their material properties are similar, their critical lengths should be similar as well (as indeed measured), even though their external diameters are apart by a factor of more than 2 (Table 2 in the main text). Note how small the effective diameters are with respect to the CNTFs external

diameters, reflecting the substantial amount of voids inside the CNTF and the large interfacial contact, particularly in the CNTF(EG).

S4. Multilevel composite performance assessment

We seek to identify the performance trends of a multilevel composite reinforced with CNTFs, associated with the intricate cross sectional geometry of a CNTF infiltrated by a matrix. A key parameter in assessing the performance is the critical length l_c, the length above which the filler breaks under tension rather than pulls out from the matrix. Following our analysis in Section S3 and in the main text, for aligned fillers with complex cross sectional shapes including gaps, voids, and matrix penetration, l_c is given by combining the inverted form of equation (S15) with equation (S19) (or equations (2) and (3) in the main text):

$$l_c = \frac{\sigma_f \langle D \rangle}{2\tau}, \quad \langle D \rangle = \frac{4a}{p} = C_{td}(1-P)D. \tag{S20}$$

$\langle D \rangle$ is the filler effective diameter, and τ is the actual interfacial shear strength, assuming the matrix yields prior to debonding and flows plastically.

The contribution of the filler to the strength of a composite reinforced with an aligned filler of average length l is given by [12, 19-20]:

$$\sigma = \left[1 - \tfrac{1}{2}\left(\frac{l}{l_c}\right)^{-1}\right] V_f \sigma_f, \quad l \geq l_c, \tag{S21}$$

where V_f is the volume fraction of the filler in the composite, and σ_f is its actual material strength. The domain $l \geq l_c$ is selected since CNTFs are practically continuous fibers, and therefore their length is longer than their critical length. This equation is universal with respect to the filler cross sectional shape, so long as the geometry, expressed by the actual interfacial perimeter p and the material cross sectional area a, is represented by the function $l_c(\langle D \rangle)$ shown in equation (S20). Expressing equation (S21) in terms of the geometry factor C_{td} and matrix penetration factor P, we get:

$$\sigma = \left[1 - \frac{\sigma_f \langle D \rangle}{4\tau l}\right] V_f \sigma_f = \left[1 - \frac{\sigma_f D}{4\tau l} C_{td}(1-P)\right] V_f \sigma_f . \qquad \text{(S22)}$$

At a given V_f, smaller $\langle D \rangle$ means smaller l_c, leading to higher composite strength. In other words, more CNTF internal gaps and voids (*i.e.*, higher degree of hollowness, or smaller C_{td}), as well as higher matrix penetration inside the CNTF (larger P), enhance the composite strength. As demonstrated in our experiments and analysis, $\langle D \rangle$ can be smaller than D by a factor of about 4 ($C_{td} \cong 0.25$) due to the CNTF's internal gaps and voids, as well as by an additional factor of about 2 ($P \cong 0.5$) due to matrix penetration.

The composite toughness in terms of pullout energy, the energy absorbed during fracture when a filler is pulled out from a matrix, is given by [12]:

$$G = \frac{V_f \sigma_f l_c}{12} \left(\frac{l}{l_c}\right)^{-1}, \quad l \geq l_c . \qquad \text{(S23)}$$

This equation is universal with respect to the filler cross sectional shape, since the geometry is incorporated in the function $l_c(\langle D \rangle)$ (equation (S20)). As already mentioned, $l \geq l_c$ is the relevant domain for the long CNTFs. Expressing equation (S23) in terms of the geometry factor C_{td} and matrix penetration factor P, we get:

$$G = \frac{V_f \sigma_f^3 \langle D \rangle^2}{48\tau^2 l} = \frac{V_f \sigma_f^3 D^2}{48\tau^2 l} C_{td}^2 (1-P)^2 . \qquad \text{(S24)}$$

Smaller $\langle D \rangle$ means smaller l_c, leading to lower composite toughness, in other words, higher degree of hollowness CNTF (smaller C_{td}) and higher matrix penetration (larger P) degrade the composite toughness. However, this negative effect of an interphase on toughness could be offset by increasing the CNTF diameter D accordingly, without changing the filler volume fraction, and with a moderate cost in the composite strength. As demonstrated in our experiments, although the CNTF(EG) had a much higher effective interfacial strength, its critical length matched that of the CNTF(HNO_3) owing to its larger diameter (Table 2 in the main text).

Hence, when an aligned long filler is used for reinforcement, a shorter l_c increases the composite strength yet weakens its toughness, and vice versa, where the toughness is expressed

in terms of the energy absorbed by pulling out CNTFs from the matrix during fracture [12, 19-20]. In other words, more CNTF internal gaps and voids (*i.e.*, higher degree of hollowness, or smaller C_{td}), as well as higher matrix penetration inside the CNTF (larger P), enhance the composite strength, while degrading its toughness, and vice versa. At the same time, toughness can be improved by increasing the CNTF diameter D, with a moderate cost in the composite strength.

In addition to the CNTF volume fraction, when matrix penetration occurs a second volume fraction may be introduced, to account for the amount of CNTs or CNT bundles in contact with the matrix inside the CNTF. We designate these two volume fractions as external and internal, V_f^{ext} and V_f^{int}, respectively, so that the overall filler volume fraction is given by:

$$V_f = V_f^{ext} V_f^{int} = \left(\frac{v_{\text{CNTF}}}{v_{\text{Composite}}} \right) \left(\frac{v_{\text{CNT}}}{v_{\text{CNTF}}} \right), \qquad \text{(S25)}$$

where v designates overall volume. This concept is illustrated in Figure S2. The internal volume fraction V_f^{int} should be close to that of tight packing (≤ 0.9 for hexagonal packing, depending on the CNTs hollowness or the aspect ratio t/d), since the matrix inside the CNTF mostly fills the existing gaps between the CNTs or CNT bundles, without expanding the CNTF overall volume.

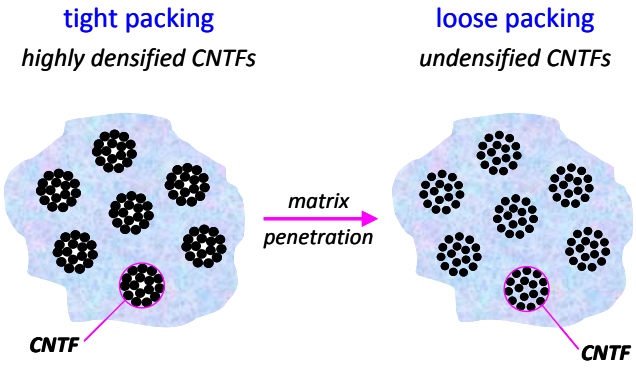

Figure S2. Illustration of filler volume fractions. Two volume fractions: an internal volume fraction of CNTs with respect to a CNTF, and an external volume fraction of CNTFs with respect to the composite.

We proceed with assessing the ranges of the parameters that determine the composite performance in accordance with equations (S21)-(S24). The performance of a composite reinforced with aligned uniformly dispersed CNTs is used as a comparison reference for assessing the performance of a composite reinforced with CNTFs. For aligned CNTs the ratio l/l_c is typically around 1 [12], whereas for aligned CNTFs $l/l_c >> 1$ since their length is practically infinite. Therefore, for the same V_f, we expect the contribution of the filler to the composite strength to be twice as high for CNTFs compared to CNTs (the term in brackets in equation (S21) approaches 1 for CNTFs, compared to 1/2 for aligned CNTs). The reason for this is that when the filler has the same length as its critical length, it does not break during fracture but rather pulls out from the matrix, whereas when the filler is much longer than its critical length, a large portion of the filler elements break rather than pull out, resulting in higher effective strength. The strength of a CNT reinforced composite can even be worse when the CNTs are randomly oriented, as is usually the case, since only a fraction of the CNTs contribute to the strength in a desired direction.

Furthermore, whereas CNTs can be dispersed uniformly only at fairly low volume fractions (~0.05-0.1) because of agglomeration [21], CNTFs can be arranged uniformly in the matrix at much higher volume fractions, since their microscale diameter enables controlled handling and composite preparation as with regular microscale fibers. We estimate the CNTF volume fraction (external volume fraction, V_f^{ext}) to be of the order of 0.6-0.8, much higher than in aligned CNTs. In addition, when matrix penetration occurs, the volume fraction of CNT bundles in a CNTF (internal volume fraction, V_f^{int}) should be considered. The internal volume fraction V_f^{int} should be close to that of tight packing (≤ 0.9 for hexagonal packing, depending on the CNTs hollowness or the aspect ratio t/d), since the matrix inside the CNTF mostly fills the existing gaps between the CNTs or CNT bundles, without expanding the CNTF overall volume. The overall filler volume fraction is estimated by equation (S25), which, using the values $V_f^{ext} \approx 0.6-0.8$ and $V_f^{int} \approx 0.7-0.8$, results in an estimate of $V_f \approx 0.4-0.6$.

Since l_c is proportional to the filler effective diameter and actual strength (equation (S20)), the critical length of a CNTF is ~10^2 higher compared to a CNTs (see data in Table 2 and Table 3 in the main text), assuming both have a length similar to their respective l_c. Therefore, in

principle, the toughness of a CNTF reinforced composite should be, for similar values of V_f and τ, about two orders of magnitude higher than a CNT reinforced composite. However, this large difference is lessened by the large l/l_c ratio in CNTFs, whose length is virtually infinite and limited in practice only by the density of critical defects along the CNTF. The reason for this is that, contrary to the strength (equation (S21)), the toughness decreases for larger values of l/l_c since a larger portion of the filler elements break rather than pull out, absorbing less energy (equation (S23)).

In addition to the energy absorbed by pulling out the whole CNTF from the surrounding matrix (external pullout energy), for CNTFs penetrated by matrix further energy is absorbed by the pullout of individual CNTs or CNT bundles from the interphase (internal pullout energy). By the same logic as before, the bundle's effective diameter (and hence its l_c) is smaller by ~10^2 compared to the CNTF effective diameter, and therefore the resulting G of a bundle (equation (S23)) should be about two orders of magnitude lower compared to a CNTF. However, the strength of an individual CNT or a CNT bundle is higher than that of a CNTF (Table 3 in the main text), lessening this difference. Additional factors (*e.g.*, l/l_c, τ, V_f, and P) should also be taken in consideration and indeed reverse the picture. These complex relationships can be clarified by writing the ratio between the internal pullout energy G_{int} and the external pullout energy G_{ext}, using equation (S24):

$$\frac{G_{int}}{G_{ext}} = \left(\frac{\sigma_{bundle}}{\sigma_{CNTF}}\right)^3 \left(\frac{\tau_{ext}}{\tau_{int}}\right)^2 \left(\frac{1-P_{bundle}}{1-P_{CNTF}}\right)^2 \left(\frac{D_{bundle}}{D_{CNTF}}\right)^2 \left(\frac{l_{CNTF}}{l_{bundle}}\right). \qquad \text{(S26)}$$

We use order of magnitude parametric values to estimate this ratio. The volume fraction V_f was omitted, since G_{int} should be normalized (*i.e.*, averaged) over the whole composite cross sectional area rather than just the CNTF area (in other words, $V_f^{int}V_f^{ext}/V_f = 1$, equation (S25)). A bundle should have a higher material strength than a complete CNTF, since at smaller scales strength is generally higher, as reflected in Table 3 and Figure 4 in the main text when comparing a CNT to a CNTF, and therefore we estimate $\sigma_{bundle}/\sigma_{CNTF} \approx 3$. To increase the internal energy absorption, we assume the CNTF is impregnated by a softer (weaker) matrix than the surrounding matrix, and use the value $\tau_{ext}/\tau_{int} \approx 3$. The geometric factor C_{td} is defined for tight

packing (equation (S14)) and is the same for a bundle and a CNTF, and therefore omitted. We take $P_{CNTF} \approx 0.5$ as assessed for our CNTF-HNO_3 experimental case in Figure S1), and $P_{bundle} \approx 0$ since the bundle is not infiltrated, and therefore we estimate $(1-P_{bundle})/(1-P_{CNTF}) \approx 2$. The CNTF diameter is ~10μm (Table 2 in the main text), and a bundle inside a CNTF has a diameter of ~0.1μm (Figure 2d in the main text), and therefore we estimate $D_{bundle}/D_{CNTF} \approx 10^{-2}$. Regarding the CNTF and bundle lengths, in the absence of specific data we estimate their ratio to be similar to that of the diameters, namely $l_{CNTF}/l_{bundle} \approx 10^{2}$. Using these values, we obtain the order of magnitude estimate $G_{int}/G_{ext} \approx 10^{1}$.

Pullout energy is also absorbed inside a CNTF when there is no interphase, as a result of the friction between CNTs. However, this energy is much lower compared to pullout from a matrix, since the van der Waals interaction between adjacents CNTs is limited to a point or a line, compared to an area when an interphase is present. The difference between these two pullout mechanisms is evidenced by the plastic flow of the matrix when an interphase is present (Figure 2a), compared to the direct tearing of CNTs in a CNTF without an interphase (Figure 2e). As demonstrated above, a small fraction of very soft interphase, introduced into the CNTF by impregnation prior to composite preparation, could increase the contribution of this internal energy component, by decreasing the interfacial shear strength between the matrix and individual CNTs or CNT bundles. This could be achieved with minimal impact on the overall strength, since at high volume fractions the strength is dominated by the strength of the CNT bundle. Such approach has also the potential to boost the fracture toughness of the embedded CNTFs, by spreading the stress more uniformly in a cross section, and by arresting crack propagation. Similar toughening mechanisms were observed in solution spun PVA fibers reinforced by CNT and graphene, which formed an interconnected partially aligned network [22].

These performance assessments are summarized in Figure 7 in the main text, using equations (S21)-(S24), mapping the strength versus the toughness of composites, for a range of the parameters V_f, σ_f, l_c and l/l_c. Based on the above parametric estimates, the following representative values were used for aligned CNTs: $V_f = 0.05$, $\sigma_f = 30$ GPa, $l_c = 3$ μm, and $l/l_c = 1$, and for aligned CNTFs: $V_f = 0.5$, $\sigma_f = 8$ GPa, $l_c = 300$ μm, and $l/l_c = 30$. In addition, an order of magnitude higher toughness was used for the infiltrated CNTFs compared to the

tightly packed CNTFs (equation (S26)). The regions depicted in Figure 7 in the main text for each reinforcement type reflect the RSS tolerance of the composite strength and toughness, when a range of ±40% was applied to each of the parameters in equations (S21)-(S26). For comparison with carbon fibers (CF), we assume: $V_f = 0.5$, $\sigma_f = 6.8\,\text{GPa}$ [23], $l_c = 200\,\mu\text{m}$, and $l/l_c = 45$.

We see a potential for about an order of magnitude improvement in both strength and toughness of the CNTFs reinforcement compared to aligned CNTs reinforcement, and a further order of magnitude improvement in toughness for the infiltrated CNTFs reinforcement. The expected composite strength is about 4 GPa, based on our measured embedded fiber strength. By comparison, dense CNT forests, aligned by mechanical rolling and impregnated with epoxy, exhibited a strength of only about 0.2 GPa [24], most probably due to lower degree of alignment and densification than that found in CNTFs. The order of magnitude improvement in toughness is in agreement with observations in solution spun PVA fibers with high CNT and graphene volume fraction [22]. We expect the composite stiffness (*i.e.,* the elastic modulus), which is not shown in the plot, to behave in a similar way as the strength. As seen in Figure 7 in the main text, the advantage of CNTF reinforcement over uniformly dispersed, aligned CNT reinforcement is evident, in both the strength and toughness, and tradeoffs between strength and toughness are possible as well. The improvement in toughness when an interphase is introduced is achieved with negligible impact on strength. Also, carbon fiber (CF) reinforcement is estimated to have a similar strength as CNTF reinforcement, but a much lower toughness compared to both tightly packed and infiltrated CNTFs.

The presence of an interphase, its type and size, is particularly significant in boosting the energy absorption during fracture, giving the EG-treated CNTF a clear advantage over the HNO_3-treated CNTF. Hence, our motivation is to be able to tune the interphase according to the engineering goals set for a particular design. Note in Figure 7 the larger performance span of the infiltrated CNTFs, compared to the tightly packed CNTFs, which reflects the wider parametric variability available by tuning the interphase. Further tuning can be achieved by modifying the degree of hollowness of the CNTF, by varying the wall thickness of the CNTs (*i.e.,* the number of CNT layers) and the gaps between CNT bundles. Finally, although this analysis shows clear performance trends for a CNTF-reinforced composite, the numerical estimates should be regarded with some caution, as some of the parameters are still uncertain at this time, such as the

stress uniformity within a CNTF (whether infiltrated or not), the properties of a CNT bundle, and practical packing densities of CNTFs.

S5. X-ray photoelectron spectroscopy (XPS)

The chemical composition of the CNTFs was investigated using XPS. By turning on the eFG, specimen signals are differentiated from those of the supporting glass [25], thus improving significantly the reliability of the chemical quantification and the evaluation of oxygen content in particular (Figure S3). Notably, the reference sample (CNTF spun from CNT array without any densification solvent) showed significant amounts of adsorbed water and, to a lesser extent, of Si-based moieties (Table S1). Therefore, conclusions regarding differences between treated and reference CNTFs are based on both the detailed line-shape of the C 1s signal and the relevant atomic concentrations of non-carbon elements.

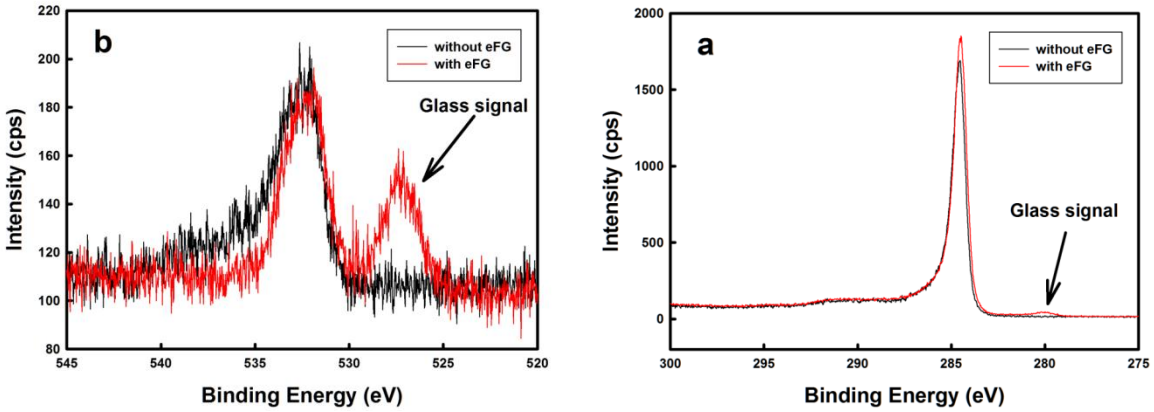

Figure S3. High resolution XPS spectra of C1s signals of CNTF (a) and O1s signals of CNTF(EG) (b). Black and red lines are the signals collected without eFG and with eFG, respectively. It clearly shows that the glass signals are separated from those of the samples with eFG turning on.

The XPS was performed on a Kratos AXIS-Ultra DLD spectrometer, using a monochromatic Al kα source at low fluxes, 15-75 W, and detection pass energies of 20-80 eV. The pressure at the analysis chamber was kept below $1 \cdot 10^{-9}$ torr. A challenge encountered in this analysis regarded the need in differentiating the CNTs-related signals from those of the substrate, where C and O contamination was rather expected. To overcome this difficulty, CNTFs (~2cm long) were stretched between two elevated holders, a few milimeters above the supporting glass

slide. The two holders were grounded, while the glass, as a strong insulator, was subject to charging during the XPS experiment. Technically, it was easy to vary the charging conditions by means of an electron flood gun (eFG), such that a high level differentiation of the desired signal could be achieved, even for the evaluation of small amounts of contaminating moieties residing on the CNTs themselves [25]. Stability of the CNTs signals was checked by repeated measurements and found to be remarkably good.

Table S1. Atomic concentrations (%) of the samples, as derived from the XPS analysis, after differentiation of the supporting glass signals (indicated separately).

	C	O	N	Si	Glass	Introduced molecule
CNTF	90.00	4.80	--	1.47	3.73	---
CNTF（EG）	90.82	3.50	--	0.66	5.02	6.0±1.6
CNTF（HNO_3）	93.42	3.76	1.22	---	1.60	

As shown in Table S1, the amount of CNTFs-related oxygen actually decreases under the EG treatment; however, the C 1s line-shape [26] clearly manifests an increase in oxidized carbon components, mainly at binding energy 286.5±0.2 eV, which can be attributed to C-OH moieties (the graphs are enlarged and inserted in Figure S4a). The slightly different charging conditions in different measurement causes shift of peaks, so the insert graphs were smoothed and shifted to have the same peak center. From the latter, we estimate the amount of EG to be ~ 6%. The possible reason for this is that the densification effect of EG forms CNT bundles in the fiber and thus reduces the surface area and adsorption of moisture from air, compared to CNTF without any treatment. Figure S4b finally shows that the oxygen signal slightly decreases during the x-ray irradiation [27], in spite of the very low fluxes used in these experiments. This is a typical artifact in XPS of reactive C-O species and, importantly, it is not observed in the reference sample. Hence, it provides an indirect indication that the EG molecules remain in a chemically reactive state.

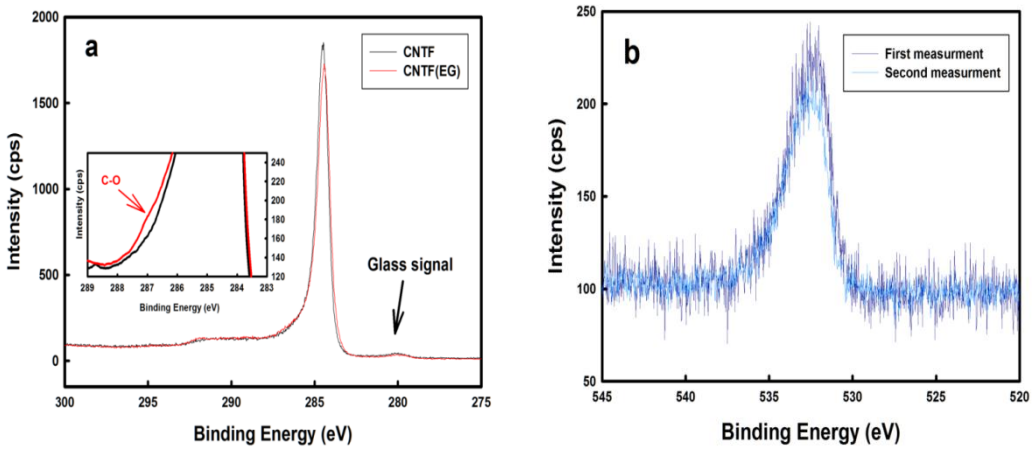

Figure S4. (a) High resolution XPS spectra of the C1s lines of CNTF without any treatment in black and CNTF (EG) in red. Part of the spectra were enlarged and inserted to show the C-O-H peak in CNTF (EG). (b) O1s lines of CNTF (EG) from different measurements, which clearly show the decrease of oxygen content due to the x-ray radiation.

For an acid treated sample, the success of HNO_3 introduction may be estimated from the N concentration, which yields ~1.2% (see Table S1). According to Meng et. al., nitric acid can oxidize CNTs and form carboxyl groups on the surface of CNTs [28]. In our study, we could not differentiate carbon of different oxidation states because the signals overlap with shake-up features. But we did observe N signal on the fiber and it is on a lower oxidation state (the N 1s binding energy is 400.0 eV), indicating that the corresponding molecules undergo chemical reaction upon insertion and, practically, no NO_3 or NO_2 groups remain.

S6. CNTF shrinkage

Under tension, the CNTF(HNO_3) shrinks radially by ~8 to 33% and detaches from the matrix, including tearing of CNT bundles (Figure 2f and h in the main text), whereas the CNTF(EG) does not appear to shrink (Figure 2c in the main text). Apparently, despite the densification process, a large amount of voids remains in the CNTF, which, if not filled with epoxy, allows diameter shrinkage under strain. A possible reason for the presence of these voids is the vacuuming step in the sample preparation process. In the CNTF(HNO_3), densification creates a shell that prevents epoxy penetration, whereas in the CNTF(EG) epoxy penetrates and fills the

voids. Another possible cause for shrinkage is the tearing and sliding of CNTs and CNT bundles during fracture, which is more pronounced in the CNTF(HNO_3) samples (Figure 2e in the main text). It is not clear whether the CNTF(HNO_3) debonding and shrinkage takes place before or after fragmentation, and whether it occurs only in the vicinity of the fracture plane. Further work is needed to clarify this failure mechanism.

References

[1] Y.N. Liu, M. Li, Y.Z. Gu, X.H. Zhang, J.N. Zhao, Q.W. Li, Z.G. Zhang, The interfacial strength and fracture characteristics of ethanol and polymer modified carbon nanotube fibers in their epoxy composites, Carbon 52 (2013) 550-558.

[2] C. Fang, J. Zhao, J. Jia, Z. Zhang, X. Zhang, Q.W. Li, Enhanced carbon nanotube fibres by polyimide, Appl. Phys. Lett. 97 (18) (2010) 181906.

[3] S. Li, X. Zhang, J. Zhao, F. Meng, G. Xu, Z. Yong, J. Jia, Z. Zhang, Q. Li, Enhancement of carbon nanotube fibres using different solvents and polymers, Compos. Sci. Technol. 72 (12) (2012) 1402-1407.

[4] T. Ohsawa, A. Nakayama, M. Miwa, A. Hasegawa, Temperature-Dependence of Critical Fiber Length for Glass Fiber-Reinforced Thermosetting Resins, J. Appl. Polym. Sci. 22 (11) (1978) 3203-3212.

[5] E.G. Stoner, D.D. Edie, S.D. Durham, An end-effect model for the single-filament tensile test, J. Mater. Sci. 29 (24) (1994) 6561-6574.

[6] B. Yavin, H.E. Gallis, J. Scherf, A. Eitan, H.D. Wagner, Continuous monitoring of the fragmentation phenomenon in single fiber composite materials, Polym. Compos. 12 (6) (1991) 436-446.

[7] H.D. Wagner, Residual stresses in microcomposites and macrocomposites, J. Adhes. 52 (1-4) (1995) 131-148.

[8] H.D. Wagner, X.F. Zhou, A twin-fiber fragmentation experiment, Compos. Pt. A-Appl. Sci. Manuf. 29 (3) (1998) 331-335.

[9] I. Miskioglu, C.P. Burger, J. Gryzagoridis, Material properties in thermal-stress analysis, N&O Joernaal (1985) 27-32.

[10] L. Deng, R.J. Young, I.A. Kinloch, R. Sun, G. Zhang, L. Noé, M. Monthioux, Coefficient of thermal expansion of carbon nanotubes measured by Raman spectroscopy, Appl. Phys. Lett. 104 (5) (2014) 051907.

[11] D. Hull, An introcuction to composite materials, Cambridge university press1981.

[12] I. Greenfeld, H.D. Wagner, Nanocomposite toughness, strength and stiffness -the role of filler geometry, Nanocomposites 1 (1) (2014) 3-17.

[13] M.F. Yu, O. Lourie, M.J. Dyer, K. Moloni, T.F. Kelly, R.S. Ruoff, Strength and breaking mechanism of multiwalled carbon nanotubes under tensile load, Science 287 (5453) (2000) 637-640.

[14] B.G. Demczyk, Y.M. Wang, J. Cumings, M. Hetman, W. Han, A. Zettl, R.O. Ritchie, Mat. Sci. Eng. A-Struct. 334 (1-2) (2002) 173-178.

[15] C.A. Cooper, S.R. Cohen, A.H. Barber, H.D. Wagner, Detachment of nanotubes from a polymer matrix, Appl. Phys. Lett. 81 (20) (2002) 3873-3875.

[16] A.H. Barber, S.R. Cohen, A. Eitan, L.S. Schadler, H.D. Wagner, Fracture transitions at a carbon-nanotube/polymer interface, Adv. Mater. 18 (1) (2006) 83-87.

[17] Y. Ganesan, C. Peng, Y. Lu, P.E. Loya, P. Moloney, E. Barrera, B.I. Yakobson, J.M. Tour, R. Ballarini, J. Lou, Interface Toughness of Carbon Nanotube Reinforced Epoxy Composites, ACS Appl. Mater. Interfaces 3 (2) (2011) 129-134.

[18] B. Coto, I. Antia, J. Barriga, M. Blanco, J.R. Sarasua, Comput. Mater. Sci. 79 (2013) 99-104.

[19] A. Kelly, W.R. Tyson, Tensile properties of fibre-reinforced metals - copper/tungsten and copper/molybdenum, J. Mech. Phys. Solids 13 (1965) 329-350.

[20] M. Piggott, Load Bearing Fibre Composites, 2nd ed., Kluwer Academic Publishers2002.

[21] J.N. Coleman, U. Khan, W.J. Blau, Y.K. Gun'ko, Small but strong: A review of the mechanical properties of carbon nanotube-polymer composites, Carbon 44 (9) (2006) 1624-1652.

[22] M.K. Shin, B. Lee, S.H. Kim, J.A. Lee, G.M. Spinks, S. Gambhir, G.G. Wallace, M.E. Kozlov, R.H. Baughman, S.J. Kim, Synergistic toughening of composite fibres by self-alignment of reduced graphene oxide and carbon nanotubes, Nat Commun 3 (2012).

[23] N. Lachman, B.J. Carey, D.P. Hashim, P.M. Ajayan, H.D. Wagner, Application of continuously-monitored single fiber fragmentation tests to carbon nanotube/carbon microfiber hybrid composites, Comp. Sci. Technol. 72 (14) (2012) 1711-1717.

[24] M. Mecklenburg, D. Mizushima, N. Ohtake, W. Bauhofer, B. Fiedler, K. Schulte, On the manufacturing and electrical and mechanical properties of ultra-high wt.% fraction aligned MWCNT and randomly oriented CNT epoxy composites, Carbon 91 (2015) 275-290.

[25] K. Shabtai, I. Rubinstein, S.R. Cohen, H. Cohen, J. Am. Chem. Soc. 122 (2000) 4959-4962.

[26] N. Lachman, X.M. Sui, T. Bendikov, H. Cohen, H.D. Wagner, Electronic and mechanical degradation of oxidized CNTs, Carbon 50 (5) (2012) 1734-1739.

[27] E. Frydman, H. Cohen, R. Maoz, J. Sagiv, Monolayer Damage in XPS Measurements as Evaluated by Independent Methods, Langmuir 13 (1997) 5089-5106.

[28] F. Meng, J. Zhao, Y. Ye, X. Zhang, Q. Li, Carbon nanotube fibers for electrochemical applications: effect of enhanced interfaces by an acid treatment, Nanoscale 4 (23) (2012) 7464-7468.